η and η' production in $\bar{p}p$ annihilation at rest

M. Chiba,[e] T. Fujitani,[d] J. Iwahori,[a,*] M. Kawaguti,[a] M. Kobayashi,[b] S. Kurokawa,[b] Y. Nagashima,[d] T. Omori,[d,†] S. Sugimoto,[d] M. Takasaki,[b] F. Takeutchi,[c] Y. Yamaguchi,[d] and H. Yoshida[a]

[a]*Faculty of Engineering, Fukui University, Fukui 910, Japan*
[b]*National Laboratory for High Energy Physics (KEK), Tsukuba, Ibaraki 305, Japan*
[c]*Faculty of Science, Kyoto Sangyo University, Kita, Kyoto 603, Japan*
[d]*Physics Department, Osaka University, Toyonaka, Osaka 560, Japan*
[e]*Physics Department, Tokyo Metropolitan University, Setagaya, Tokyo 152, Japan*
(Fukui–KEK–Kyoto Sangyo–Osaka–Tokyo Metropolitan Collaboration)
(Received 12 August 1988; revised manuscript received 3 February 1989)

From measurement of $\eta \to 2\gamma$ emitted in $\bar{p}p$ annihilation at rest, we have derived the yield, or its upper limit, of annihilation into two mesons $\bar{p}p \to \eta M$ for $M = \phi$, η', ω, ρ^0, η, and π^0/γ (sum of π^0 and γ), the branching ratio of the inclusive η production $\bar{p}p \to \eta X$ for different charge multiplicities of X, and the inclusive η/π^0 ratio. An upper limit for the inclusive η' production $\bar{p}p \to \eta' X$ has also been obtained.

I. INTRODUCTION

Study of $\bar{p}p$ annihilation at rest gives us useful information on quark dynamics in nucleons. Since $\bar{p}p$ annihilation is a short-range process of a large number of quarks and antiquarks caused by the overlap of $\bar{p}$ and p wave functions, the analysis has been usually carried out phenomenologically at quark levels. Among the phenomenological models, the quark-line-rule (QLR) approaches[1–9] have attracted much attention in these years. Dominance of quark-rearrangement or quark-annihilation graphs (see Fig. 1) has been investigated by comparing experimental branching ratios into various channels with calculation.

Annihilation into three mesons was first calculated in quark-rearrangement models;[1,2] a qualitative agreement with experimental result was obtained for many channels. Later, an alternative model in terms of annihilation and creation of quark pairs was proposed.[3,4] Taking the annihilation and creation vertices of quark pairs with the vacuum quantum number (the $^3P_0$ model), Maruyama, Furui, and Faesler[4] showed that the annihilation graph ($A3$ in Fig. 1) gives better agreement with experimental data than the rearrangement graph ($R3$) though the preference of $A3$ is not conclusive. For example,[4] annihilations into $f\pi^+\pi^-$ and $A_2^0\pi^+\pi^-$ have been experimentally observed, in consistency with the annihilation model while they are forbidden in the rearrangement model.

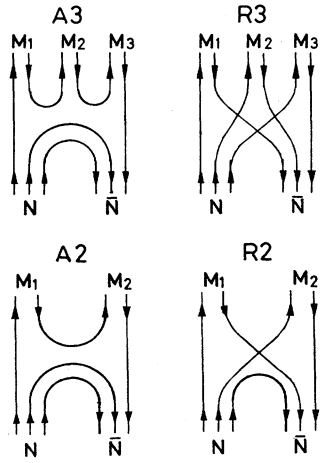

FIG. 1. Quark-annihilation graphs for $\bar{p}p$ annihilation into three mesons($A3$) and two mesons($A2$), and quark-rearrangement graphs into three mesons($R3$) and two mesons($R2$).

Annihilation into two mesons was also calculated in both quark-rearrangement and quark-annihilation models.[3,5–8] Similar to the case of annihilation into three mesons, dominance of rearrangement or annihilation models has not yet been decisive. Only qualitative preference of the annihilation models has been claimed on the basis of some experimental data, for example, much smaller branching ratio for $\bar{p}p \to \rho\rho$ than for $\bar{p}p \to \pi\rho$ (Ref. 3), sizable branching ratios for $\bar{p}p \to \pi\rho$, πA_2, etc. (Refs. 8 and 9). On the other hand, importance of the rearrangement graph has also been pointed out on the basis of, for example,[5] a sizable ratio of $\bar{p}p \to \pi^0\eta/\pi^0\pi^0$, suppression of $K^+K^-/\pi^+\pi^-$ ratio for the P-wave initial state, etc. As shown above, it is not yet conclusive which graph dominates $\bar{p}p$ annihilation at rest; preference of $A3$ and $A2$ graphs (planar-graph dominance) is still at a qualitative stage. One of the reasons why the conclusion remains indefinite is the shortage of precise data and even lack of any data in some important channels.

Experimental branching ratios into channels including η or η' are scarce, though they are important in settling the problems mentioned above. Comparison among $\bar{p}p \to \pi^0\pi^0$, $\pi^0\eta$, $\eta\eta$, $\pi^0\eta'$, $\eta'\eta'$, etc., may give important information on the dominance of quark-rearrangement or quark-annihilation graphs, as discussed by Dover and

Fishbane,[5] Genz,[6] and Hartman, Klempt, and Korner.[7] Topological branching ratio of inclusive η (η') production $\bar{p}p \to \eta(\eta')X$ with respect to the charge multiplicity of X is also important experimental information. Genz[10] showed that branching ratios for $\bar{p}p \to M_1 M_2$ with M_1 and M_2 any of π^0, η, and η' provide an independent determination of the pseudoscalar mixing angle θ_{PS}, which has usually been determined from the mass formula.

In this experiment, we have measured $\eta \to 2\gamma$ decay emitted in $\bar{p}p$ annihilation at rest and derived branching ratios of $\bar{p}p \to \eta\omega$, $\eta\rho^0$, and $\eta\pi^0/\gamma$ (sum of $\eta\pi^0$ and $\eta\gamma$), upper limits for $\eta\phi$, $\eta\eta'$, and $\eta\eta$, the branching ratio of $\bar{p}p \to \eta X$ (X denoting anything) for different charge multiplicities of X, and the inclusive η/π^0 ratio. An upper limit for η' production has also been obtained.

II. EXPERIMENT

The experimental setup was already described in Ref. 11; only its central part is sketched in Fig. 2. Antiprotons at 580 MeV/c, produced by an external beam of the KEK 12-GeV proton synchrotron, were slowed down in a graphite degrader, tracked in circular multiwire proportional chambers (MWPC's) and finally stopped in a liquid-hydrogen target of 14 cm in diameter and 23 cm in length. γ rays were measured with two detectors: a large array of NaI(Tl) modules[12] which were assembled in a half-barrel configuration and surrounded by a scintillating glass wall, and a small array of bismuth germanate (BGO, $Bi_4Ge_3O_{12}$) modules[13] which were surrounded by an NaI(Tl) wall. The two detectors covered effective acceptances of 22% and 1.3% of 4π sr, respectively, and were placed opposite to each other with respect to the target. Charged particles were tracked with cylindrical as well as flat MWPC's, whose total coverage was 93% of 4π sr. Actual tracking efficiency was a little smaller (about 90%) due to small inefficiency of the wire planes. Hodoscopes of plastic scintillator, cylindrical as well as planar in their shapes, served for triggering. The cylindrical hodoscope composing 36 scintillator slabs extended along the beam axis. The triggering condition was the existence of one or two γ rays above a threshold of 20 MeV on the NaI (NaI trigger) or at least one γ ray above 40 MeV on the BGO (BGO trigger). A fast cluster-counting logic circuit[14] selected events to be triggered.

We estimated[14] the effective energy resolution of the NaI by measuring the 129-MeV Panofsky γ rays, which were produced in calibration runs by stopping a π^- beam in the liquid-hydrogen target. When the same software cluster-finding logic as used for baryonium search[11] was applied, a full width at half-maximum (FWHM) resolution was 10.4%. Assuming $E^{-1/4}$ dependence on the γ energy E we took the overall energy resolution as

$$\Delta E/E = 0.062/(E \text{ in GeV})^{1/4} \text{ in FWHM} . \quad (1)$$

The BGO detector was simpler since, due to its small size of approximately 14 cm×17 cm×20 cm (in depth), no sophisticated cluster-counting logic was used. The effective energy resolution was again estimated from measurement of the 129 MeV γ rays to be

$$\Delta E/E = 0.068/(E \text{ in GeV})^{1/4} \text{ in FWHM} . \quad (2)$$

The gain of each γ module was monitored[14] with an accuracy of 1% throughout the experiment and corrected for in the software analysis. The energy scale was calibrated to within 2% for the NaI both with the 129 MeV γ rays and with 780 MeV π^0 from $\bar{p}p \to \pi^0\rho^0/\omega$, and to within 4% for the BGO with the 129 MeV γ rays.

III. DATA REDUCTION

From 3.6×10^7 triggered events in total, we first removed spurious incident beam events: namely, bunched beam events, events with spurious hits in the beam MWPC's, etc. We further required the existence of a slow antiproton track downstream of the degrader. For

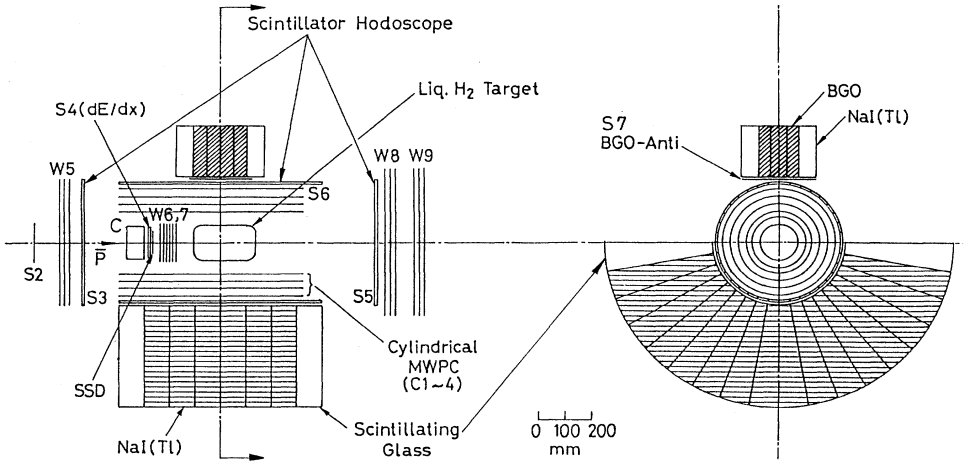

FIG. 2. Sketch of the experimental setup. $S1$ (not shown) and $S2$ for the time-of-flight measurement, $S4$ for dE/dx measurement and $S7$ for anticoincidence against charged particles entering BGO, are all of plastic scintillators, C is a graphite degrader of 13.2 g/cm^2 thickness.

the 2.7×10^7 accepted events, the vertex was reconstructed from the primary as well as the secondary charged tracks. If the final state did not include any charged particles, the vertex was determined from the track of the projectile antiproton and its dE/dx in a 3-mm-thick Si solid-state detector. The vertex reconstruction was successful for 1.7×10^7 events after the following requirements: (i) the rms distance from the vertex to the charged tracks should be less than 3 cm, and (ii) the vertex should not be located outside the target cell by more than 0.5 cm either radially or longitudinally.

Gamma rays were identified by energy deposits in the γ detectors and by the absence of signals in the scintillator hodoscope as well as in the MWPC in front of the hit NaI modules. As the particle multiplicity in the large NaI detector was frequently more than one, a cluster-finding logic[14] was applied to isolate each energy cluster from neighboring ones. Each cluster was then divided into particles, if it comprised more than one particle. For the obtained γ rays, we further required that shower leakage into the scintillating glass (for the NaI detector) or into the NaI (for the BGO) should be less than 10% of the γ energy. After the above processing, the total number of γ rays above 10 MeV, $N\gamma$ was 1.57×10^7 in the NaI and 5.21×10^5 in the BGO.

Some events involved no or more than two γ rays in the NaI. Event distribution with respect to the γ-ray multiplicity was as follows: 29.6% for no γ, 51.0% for 1γ, 17.1% for 2γ, 2.1% for 3γ, and 0.2% for $\geq 4\gamma$. For events with more than one γ ray in the NaI and the BGO, the invariant mass of two γ rays, $M(\gamma\gamma)$, was calculated for all possible combinations in the same way as described in Ref. 15. Two different topologies for $(\gamma\gamma)$ combinations were possible: in one topology, both γ rays fell on the NaI [we call this topology NaI(2γ) throughout this paper], and in the other topology, one γ fell on the NaI and the other on the BGO [NaI(1γ)+BGO(1γ)]. The $M(\gamma\gamma)$ spectra for the NaI(2γ) (4.16×10^6 combinations) and for the NaI(1γ)+BGO(1γ) (2.26×10^5) are presented in Figs. 3 and 4, respectively. The spectra are given separately for each charge multiplicity in the final state, $N_{\rm ch}$. Events with $N_{\rm ch}=1$, 3, and 5 occurred mainly from tracking inefficiency or from $\gamma\rightarrow e^+e^-$ conversion. They were simply added to events with $N_{\rm ch}=2$, 4, and 6, respectively. The η peak is clearly seen at 548 MeV for NaI(2γ) and 554 MeV for NaI(1γ)+BGO(1γ). The number of η was determined by fitting the $M(\gamma\gamma)$ spectra with a polynomial background plus a Gaussian type by using the minimization program MINUIT (Ref. 16). When summed over $N_{\rm ch}$, the number of η was 1.15×10^4 for NaI(2γ), and 2.50×10^3 for NaI(1γ)+BGO(1γ).

The $\gamma\gamma$ invariant-mass resolution is related to those of two γ energies k_1 and k_2 and of the opening angle θ between the two γ rays in the following way:

$$\frac{\sigma(M(\gamma\gamma))}{M(\gamma\gamma)}=\frac{1}{2}\left[\left[\frac{\sigma(k_1)}{k_1}\right]^2+\left[\frac{\sigma(k_2)}{k_2}\right]^2+\left[\frac{\sin\theta\sigma(\theta)}{1-\cos\theta}\right]^2\right]^{1/2}, \tag{3}$$

where the rms error $\sigma(k)$ is given by Eqs. (1) or (2). The rms angular error $\sigma(\theta)$ was estimated in a Monte Carlo simulation to be a few to several degrees depending on the incident angles of γ rays to the calorimeter. Since θ was larger than 65.2°, which occurred in the reaction $\bar{p}p\rightarrow\eta\gamma$, the $\sigma(\theta)$ term was comparable to or even larger than the $\sigma(k_1)$ and $\sigma(k_2)$ terms, unless θ was much larger than 90°. The rms width of the η peak was about 30 MeV for NaI(2γ) (see Fig. 3) and 27 MeV for NaI(1γ)+BGO(1γ) (see Fig. 4) in consistency with Eq. (3).

The number of stopped antiprotons $N_{\bar{p}}$ is related to $N\gamma$ by

$$N_{\bar{p}}\kappa\int\rho(E)\eta(E)dE=N\gamma\ , \tag{4}$$

where $\rho\,dE$ is the number of γ rays with energies between E and $E+dE$ per annihilation, η the detection efficiency of γ rays, and κ the correction factor for contamination of fake γ rays (unseparated two γ rays from π^0 decay, single γ rays mistaken as two γ rays owing to shower spread, etc.). From a Monte Carlo simulation,[14] we obtained $\kappa=1.081$ and $\int\rho\eta\,dE/\int\rho\,dE=0.1254$ for the NaI detector. Here $\int\rho\,dE$, the multiplicity of γ rays per annihilation was taken as 3.93 (Ref. 17). Substitution of these values together with $N\gamma$ in NaI into Eq. (4) gave $N_{\bar{p}}=2.94\times10^7$. Though an independent estimation of $N_{\bar{p}}$ is possible from the BGO sector, the precision in η may be poorer for the BGO than for the NaI due to the small size of the BGO detector. Consequently, we did not use the number of γ rays in the BGO to estimate $N_{\bar{p}}$ but, on the contrary, used it to determine the effective geometrical acceptance of the BGO detector by using the $N_{\bar{p}}$ obtained from the NaI sector.

IV. Result

A. Annihilation into two mesons

In order to measure the yields of exclusive annihilation channels $\bar{p}p\rightarrow\eta M$ for $M=\phi$, η', ω, ρ^0, η, and π^0/γ (sum of π^0 and γ), we first selected η samples imposing a $\gamma\gamma$ invariant-mass cut of $\pm2.0\sigma$. The energy spectra of the η samples are presented in Fig. 5 for NaI(2γ) and in Fig. 6 for NaI(1γ)+BOG(1γ). The η sample includes, in addition to true η, 3–6 times of background (see Figs. 3 and 4) depending on the charge multiplicity in the decay of M and on the detector topology (the NaI only or the NaI-BGO combination). We can determine the yield of the exclusive channels from monochromatic peaks in the η energy spectra, since the background 2γ rays should not create monochromatic peaks.

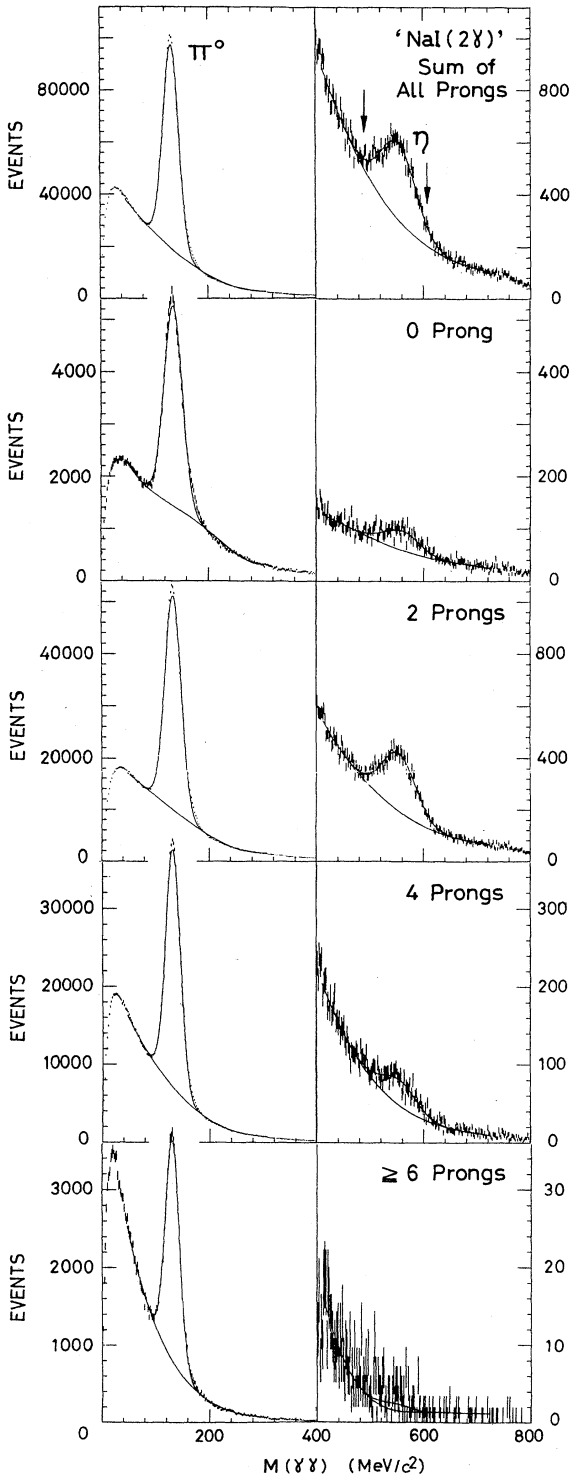

FIG. 3. Invariant-mass spectra of two γ rays for the NaI(2γ) events are presented for the sum over the charge multiplicity (top graph) and for each charge multiplicity separately. The bin width is 2.08 MeV. Solid curves represent the fit for η and π^0. Arrows indicate the cut positions for selecting η mesons. The vertical scale is different between the left and the right halves.

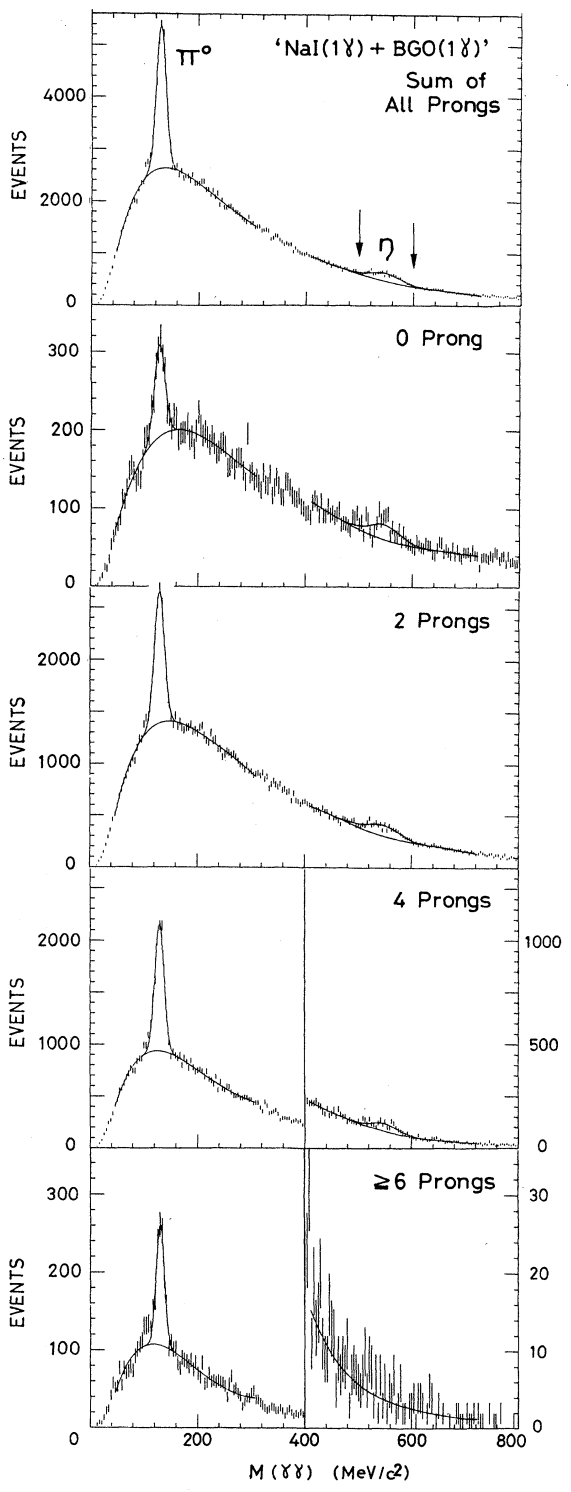

FIG. 4. Invariant-mass spectra of two γ rays for the NaI(1γ)+BGO(1γ) events. The bin width is 4.16 MeV. In the two spectra from the bottom, the vertical scale is different between the left and the right halves. Other items are the same as in the caption for Fig. 3.

Let A be the peak area (in number of events) above the background, then the yield Y of $\bar{p}p \rightarrow \eta M$ per annihilation can be obtained by the following formula:

$$N_{\bar{p}} Y \epsilon_M B(M \rightarrow N_{\rm ch}) B(\eta \rightarrow 2\gamma) = A \ , \quad (5)$$

where ϵ_M is the effective detection efficiency for $\bar{p}p \rightarrow \eta M$ with $\eta \rightarrow 2\gamma$, $B(M \rightarrow N_{\rm ch})$ the decay branching ratio of M into $N_{\rm ch}$-pronged states, and $B(\eta \rightarrow 2\gamma)$ the decay branching ratio of $\eta \rightarrow 2\gamma$ (39%). To calculate ϵ_M (see Table I), we first estimated the corresponding quantity for each decay mode of M by correcting the geometrical acceptance for the experimental condition and then took a weighted average of the quantities over the decay modes of M. The geometrical acceptance for $\eta \rightarrow 2\gamma$ is plotted in Fig. 7 versus the η energy. The corrections were calculated by a Monte Carlo simulation for (i) the

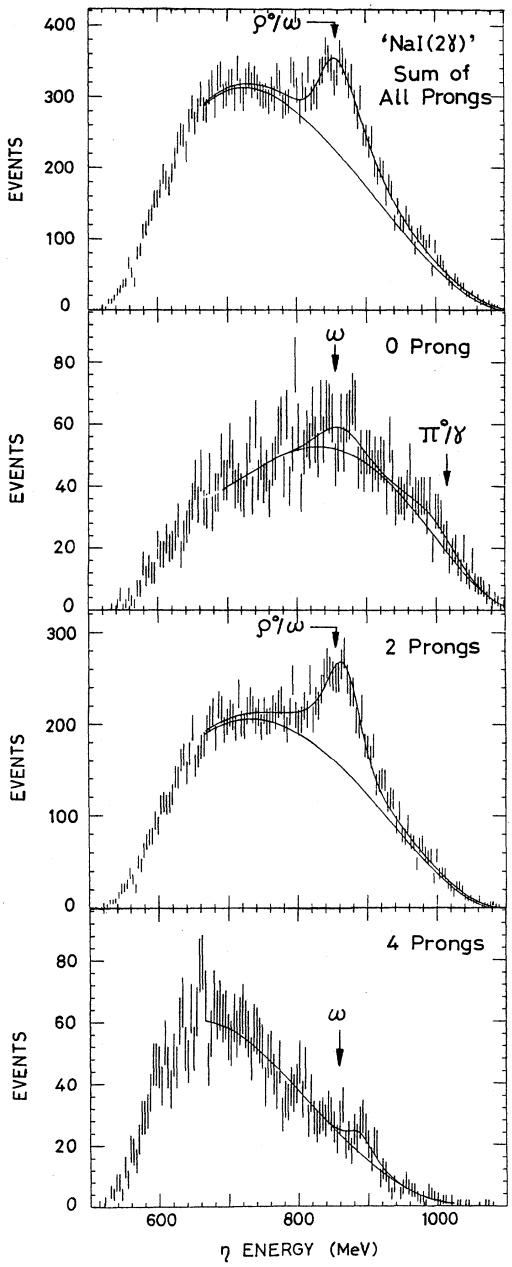

FIG. 5. Inclusive η energy spectra obtained for the NaI(2γ) events. The bin width is 4.16 MeV. The η mesons were selected by the mass cut indicated in Fig. 3 and include background as well as true η's. For the solid curve, see the text. Arrows show expected positions for $\bar{p}p \rightarrow \eta M$ for various mesons M.

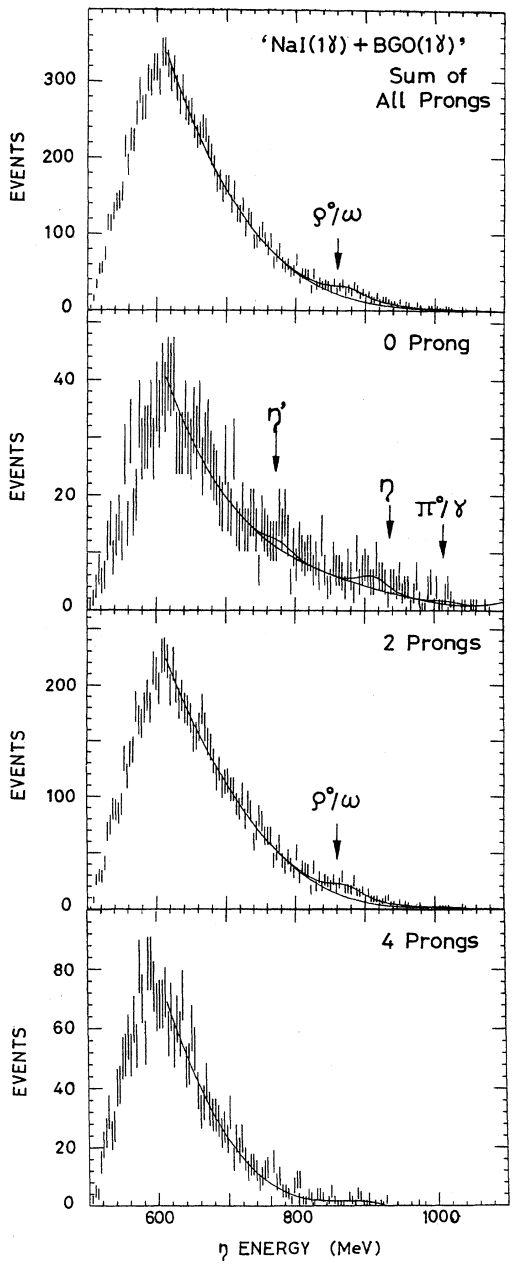

FIG. 6. Inclusive η energy spectra obtained for the NaI(1γ)+BGO(1γ) events. The η mesons were selected by the mass cut indicated in Fig. 4. Other items are the same as in the caption for Fig. 5.

TABLE I. Detection efficiency for $\eta \to 2\gamma$ produced in $\bar{p}p \to \eta M$ with M decaying into N_{ch}-pronged states. B (uncorrected) gives the decay branching ratio into N_{ch}-pronged state. B (corrected) gives the branching ratio corrected for $\gamma \to e^+e^-$ conversion and inefficiency in wire planes. The quoted errors are due to an ambiguity in the Monte Carlo calculation.

Reaction	η Energy (MeV)	N_{ch}	B (uncorrected)	B (corrected)	Detection efficiency (%) NaI(2γ)	NaI(1γ)+BGO(1γ)
$\bar{p}p \to \eta\phi$	743	0[a]	11.9%	10.2%	1.32±0.07	0.278±0.020
		2[a]	88.1%	88.1%	1.65±0.17	0.323±0.066
$\bar{p}p \to \eta\eta'$	772	0	17.7%	12.7%	0.97±0.15	0.130±0.020
		2	69.7%	64.0%	1.52±0.46	0.226±0.087
		4	12.6%	21.9%	1.19±0.23	0.156±0.026
$\bar{p}p \to \eta\omega$	852	0	8.7%	7.6%	2.30±0.14	0.195±0.010
		2	91.3%	82.0%	1.77±0.18	0.135±0.014
		4		10.4%	1.77±0.18[b]	0.135±0.014[b]
$\bar{p}p \to \eta\rho^0$	858	2	100%	99.5%	2.37±0.12	0.203±0.010
$\bar{p}p \to \eta\eta$[c]	938	0	70.9%	56.4%	5.39±0.26	0.247±0.012
		2	29.1%	40.4%	4.08±0.43	0.174±0.017
$\bar{p}p \to \eta\pi^0$	1014	0	100%	88.4%	3.58±0.18	0.125±0.006
$\bar{p}p \to \eta\gamma$	1019	0	100%	94.0%	3.87±0.20	0.125±0.006

[a]Decay of K^+, K^-, and K_L was assumed to be negligibly small.
[b]The detection efficiency for $N_{ch}=4$ was assumed to be the same as for $N_{ch}=2$ since the same decay products were detected except for the effect of $\gamma \to e^+e^-$ conversion.
[c]The detection efficiencies listed are already doubled corresponding to the existence of two η mesons.

trigger condition (see Sec. II), (ii) overlap of γ rays with charged particles, and (iii) loss of γ rays due to $\gamma \to e^+e^-$ conversion (about 6% per γ ray). $B(M \to N_{ch})$ (see Table I) was also corrected for $\gamma \to e^+e^-$ conversion and inefficiency in wire planes.

To obtain the peak area, we fitted the η energy spectrum with a polynomial background plus narrow peaks located near the expected energies. The fitting was done in various energy windows with the range up to 500 MeV. Polynomials of order 4 were sufficient to give the χ^2 divided by the degree of freedom as small as unity. The instrumental energy resolution for η must be close to but better than that for γ rays if the energies are equal. Consequently we used Eq. (1) with E that read as η energy. The energy resolution of η was bound within the instrumental width ±20%. The fitted result is shown in Figs. 5 and 6 with solid curves and is summarized in Table II. The quoted error came from the larger of the MINUIT error and the statistical ambiguity of the amount of the background lying under the peak within ±instrumental FWHM. Only $\bar{p}p \to \eta\rho^0/\omega$ showed a significant peak (10σ effect), while the other channels showed no or less than 2σ peaks.

The yield, which is also called the branching ratio B below, was calculated according to Eq. (5) for each of NaI(2γ) and NaI(1γ)+BGO(1γ) topologies and the result is given in Table III. Taking statistical average of the results from the both topologies, we obtained the final result

$$B(\bar{p}p \to \eta\phi) < 2.8 \times 10^{-3} \quad (95\%\ \text{C.L.}) , \tag{6a}$$

$$B(\bar{p}p \to \eta\eta') < 2.3 \times 10^{-3} \quad (95\%\ \text{C.L.}) , \tag{6b}$$

$$B(\bar{p}p \to \eta\omega) = (4.6 \pm 1.4) \times 10^{-3} , \tag{6c}$$

$$B(\bar{p}p \to \eta\rho^0) = (9.6 \pm 1.6) \times 10^{-3} , \tag{6d}$$

$$B(\bar{p}p \to \eta\rho^0/\omega) = (1.4 \pm 0.2) \times 10^{-2} , \tag{6e}$$

$$B(\bar{p}p \to \eta\eta) < 7.5 \times 10^{-4} \quad (95\%\ \text{C.L.}) , \tag{6f}$$

$$B(\bar{p}p \to \eta\pi^0/\gamma) = (2.9 \pm 1.5) \times 10^{-4} . \tag{6g}$$

In the following, we give a few comments regarding the derivation of the above result.

For $\bar{p}p \to \eta\omega$, a yield of $(4.6 \pm 1.4) \times 10^{-3}$ was deduced from monochromatic peaks observed both in the zero-prong spectrum (corresponding to $\omega \to \pi^0\gamma$) and in the four-prong spectrum ($\omega \to \pi^+\pi^-\pi^0$ with $\gamma \to e^+e^-$ conversion). The prominent peak at the corresponding energy in the two-prong spectrum could result from contributions of both $\eta\omega$ with $\omega \to \pi^+\pi^-\pi^0$ and $\eta\rho^0$ with $\rho \to \pi^+\pi^-$. We tried to separate $\eta\omega$ from $\eta\rho^0$ from the shape difference of the η peaks: the $\eta\omega$ peak should be of a sharp Gaussian type with its width limited by the instrument, while the $\eta\rho^0$ peak must be of a broad Breit-Wigner type ($\Gamma = \Gamma_\rho M_\rho / 2M_N = 62.8$ MeV, here M_ρ and M_N being ρ and nucleon rest masses, respectively) folded in the resolution. The quality of the fit of the $\eta\rho^0/\omega$ peak with a sum of $\eta\rho^0$ and $\eta\omega$ hardly depended on the $\eta\omega$ yield as long as it is small. However, the quality of the fit was degraded when the $\eta\omega$ yield exceeded 9×10^{-3}. As the $\eta\omega$ yield increased, the $\eta\rho^0$ yield decreased, keeping the sum of them almost constant. The same situation as above was found both for NaI(2γ) and for NaI(1γ)+BGO(1γ). The upper limit for $\eta\omega$ obtained in this way was consistent with the $\eta\omega$ yield obtained from the zero- and four-prong spectra. Since we could not separate $\eta\omega$ from $\eta\rho^0$ precisely enough in the two-prong spectrum, we fixed the $\eta\omega$ yield at the value obtained

from the zero- and four-prong spectra and obtained a yield of $(9.6\pm1.6)\times10^{-3}$ for $\eta\rho^0$ from the average of its maximum (obtained from the fit with the $\eta\omega$ yield $=3.2\times10^{-3}$) and minimum (with 6.0×10^{-3}). The quoted error covers both the maximum and the minimum. Though the statistical and fitting ambiguity was much smaller for the sum of $\eta\omega$ and $\eta\rho^0$ than for each of $\eta\omega$ and $\eta\rho^0$, we took into account the systematic ambiguity (see Sec. V) and obtained a yield of $(1.4\pm0.2)\times10^{-2}$ for the sum of $\eta\omega$ and $\eta\rho^0$.

For $\bar{p}p\to\eta\pi^0$, separation of $\bar{p}p\to\eta\pi^0$ (at the η energy of 1014 MeV) from $\bar{p}p\to\eta\gamma$ (1019 MeV) was difficult. Since the detection efficiencies for $\eta\pi^0$ and $\eta\gamma$ were close to each other, we could obtain a yield of $(2.9\pm1.5)\times10^{-4}$ for the sum of $\eta\pi^0$ and $\eta\gamma$ from a small peak appearing in the zero-prong spectrum.

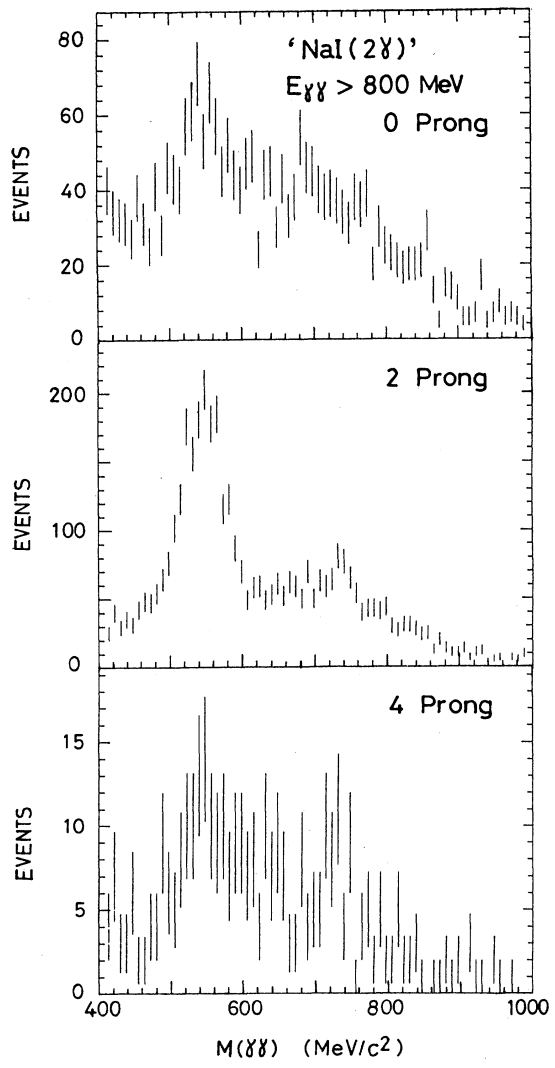

FIG. 7. Invariant-mass spectra of two γ rays with the topology of NaI(2γ) and with the sum of energies, k_1+k_2, above 800 MeV are given separately for each charge multiplicity. The bin width is 8.32 MeV. About $\frac{1}{5}$ of the total sample is included in the figure.

For $\bar{p}p\to\eta\phi$, $\eta\eta'$, and $\eta\eta$, the absence of peaks at the expected energies of 743 MeV (for $\eta\phi$), 772 MeV ($\eta\eta'$), and 938 MeV ($\eta\eta$) gave the upper limits for the yield. These channels can be suppressed by the Okubo-Zweig-Iizuka (OZI) rule[18] for $\eta\phi$ or by inhibition of S-wave annihilation in $\eta\eta'$ and $\eta\eta$. When more than one upper limit existed from the spectra with different charge multiplicities, we simply took the lowest value of them. When an upper limit was obtained from one of NaI(2γ) and NaI(1γ)+BGO(1γ) topologies and a finite number from the other, both of them were statistically combined.

A finite yield was obtained for each channel of $\bar{p}p\to\eta\omega$, $\eta\rho^0$, and $\eta\pi^0/\gamma$ as given in Eq. (6). In obtaining the result, the NaI(2γ) data were statistically more important than the NaI(1γ)+BGO(1γ) ones. The η energies are larger than 800 MeV for the above channels. Figure 7 gives invariant-mass spectra of high energy, two γ rays with k_1+k_2 above 800 MeV for the topology of NaI(2γ). A clean η peak can be seen for each charge multiplicity at approximately the same position. The peak position and the width remain essentially unchanged by selecting high-energy η candidates (compare Fig. 7 with Fig. 3). This fact indicates that there exists neither important calibration error nor resolution degradation at high energies, and that we have true high-energy η samples. The situation was qualitatively similar also for NaI(1γ)+BGO(1γ).

B. Inclusive η production $\bar{p}p\to\eta X$ for different charge multiplicities of X

The yield Y was deduced from the area A of the η peak above the background in the $M(\gamma\gamma)$ spectrum according to the following formula:

$$N_{\bar{p}}\,Y\epsilon(\bar{p}p\to\eta X)B(\eta\to2\gamma)=A\ , \tag{7}$$

where $\epsilon(\bar{p}p\to\eta X)$ is the effective detection efficiency for $\eta\to2\gamma$. Before estimating $\epsilon(\bar{p}p\to\eta X)$, we calculated the corresponding quantity for each exclusive channel, in a similar way to ϵ_M described in Sec. IV A, by folding the geometrical acceptance for $\eta\to2\gamma$ (Fig. 8) in the η energy distribution and by correcting the result for the experimental condition. We took the energy distribution of η given by the Lorentz-invariant phase space (see Fig. 9). The detection efficiencies before and after the corrections are given in Table IV. We did not include the decay $\bar{p}p\to\eta\bar{K}K+$pions, since its branching ratio is expected to be much less than that of kaonless decay.[19]

$\epsilon(\bar{p}p\to\eta X)$ for a fixed charge multiplicity of X cannot be precisely calculated unless the composition of X is known. However, it can be calculated under an assumption of single channel dominance for X. Table V gives the result of such a calculation. Since we used two independent topologies [NaI(2γ) and NaI(1γ)+BGO(1γ)] in measuring two γ rays from η, we have one more constraint that both yields obtained from the two topologies should agree with each other. This allows us to include one more channel in X and to adjust their relative yields.

TABLE II. Experimental result on narrow peaks in the inclusive η spectra. The peak position, the number of events in the peak, statistical significance, and the width (1σ) are given. Except for the $\eta\rho^0$ peak, the peaks were fitted with Gaussians, whose width was bound within the instrumental width ±20%. The width error in parentheses indicatess that the width was fitted on its upper or lower limit. For the $\eta\rho^0/\omega$ peak, see the footnote. The averaged peak position is given in the notes. No narrow peak was seen for the charge multiplicity ≥ 6.

		Charge multiplicity (N_{ch})			
	N_{ch}=all	0	2	4	Notes
		NaI(2γ)			
Position (MeV)	861±3	871±11	869±3	896±4	872±2
Events	3194±300	126±61.9	3119±229	86±36	$\bar{p}p\to\eta\rho^0/\omega$
Stat. Sig.	10.6σ	2.0σ	13.6σ	2.4σ	
Width (MeV)	a	27.6(−8.4, +0)	a	18.6(−0, +6.4)	
Position (MeV)		1004±10.0			1004±10
Events		98.7±56.0			$\bar{p}p\to\eta\pi^0/\gamma$
Stat. Sig.		1.8σ			
Width (MeV)		30.9(−9.4, +0)			
		NaI(1γ)+BGO(1γ)			
Position (MeV)		785±20			785±20
Events		14.3±18.2			$\bar{p}p\to\eta\eta'$
Stat. Sig.		0.8σ			
Width (MeV)		17.0(−0, +7.8)			
Position (MeV)	884±8		883±19		884±7
Events	345±97		318±94		$\bar{p}p\to\eta\rho^0/\omega$
Stat. Sig.	3.6σ		3.4σ		
Width (MeV)	a		a		
Position (MeV)		920±8			920±8
Events		25.9±13.1			$\bar{p}p\to\eta\eta$
Stat. Sig.		2.0σ			
Width (MeV)		19.3(−0, +6.7)			
Position (MeV)		1027±17			1027±17
Events		7.0±7.5			$\bar{p}p\to\eta\pi^0/\gamma$
Stat. Sig.		1.0σ			
Width (MeV)		20.9(−0, +8.9)			

[a]As the fit did not give a unique value for the $\eta\omega$ yield but its upper limit, a yield of 4×10^{-3} was assumed in this table [740 events for $N_{ch}=2$ and 810 events for the sum over N_{ch} for NaI(2γ), while 57 events for $N_{ch}=2$ and 62 events for the sum over N_{ch} for NaI(1γ)+BGO(1γ)]. The $\eta\omega$ peak had a Gaussian shape with the instrumental width and the $\eta\rho^0$ had a Breit-Wigner shape folded in the instrumental resolution.

Therefore, when there are only two dominant channels for the fixed charge multiplicity, we can derive the total η yield for that charge multiplicity. In a case when there are three dominant channels for the fixed charge multiplicity, we can derive the total η yield if the yield of the third channel is experimentally known.

For $N_{ch}(X)=0$, the argument goes as follows. First, the yield of $\bar{p}p\to\eta\pi^0$ was fixed to be $(3.9\pm1.0)\times10^{-4}$ from a statistical average over two values, i.e., $(2.9\pm1.5)\times10^{-4}$, our result given in Eq. (6g), and $(4.6\pm1.3)\times10^{-4}$ given in Refs. 15 and 20. Second, $\bar{p}p\to\eta m\pi^0$ with $m\geq4$ does not seem dominant on the analogy of $\bar{p}p\to\pi^0$'s; $\bar{p}p\to m'\pi^0$ with $m'\geq5$ is expected to be much less (of the order of 1%) than that with $m'<5$ from a measurement[21] of the γ multiplicity. It is then possible to derive the yields of the remaining two (possibly dominant) channels of $\bar{p}p\to\eta2\pi^0$ and $\eta3\pi^0$. We obtained the abundance ratio of $\eta2\pi^0/(\eta2\pi^0+\eta3\pi^0)=0.91\pm0.19$ requiring that the η yields obtained from the two topologies should agree with each other. The above ratio gives the η yield (uncorrected)$=(0.72\pm0.09)\%$. Correcting this for conversion of $\gamma\to e^+e^-$ and adding the assumed yield (together with its error) of $\eta\pi^0$, we finally obtained the η yield $=(0.97\pm0.12)\%$ and the yield of $\bar{p}p\to\eta2\pi^0=(0.84\pm0.10)\%$. An experimental data of $(0.93\pm0.3)\%$ given in Ref. 22 for the yield of $\bar{p}p\to\eta2\pi^0$ are consistent with the above result.

On the same line of consideration as above, we first assume for $N_{ch}(X)=2$ a yield of $(1.35\pm0.17)\%$ (Ref. 23) for $\bar{p}p\to\eta\pi^+\pi^-$; we have adopted this number as it has a better statistical accuracy than the other experimental values.[24] Second, $\bar{p}p\to\eta\pi^+\pi^-m\pi^0$ with $m\geq3$ is expected to be much less than that with $m<3$ on the analogy of the π^0 case; $\bar{p}p\to\pi^+\pi^-m'\pi^0$ with $m'\geq4$ is much less

TABLE III. $B(\bar{p}p \to \eta M)$ (or its upper limit at 95% C.L.) in 10^{-3} deduced from the inclusive η spectra. Two results from NaI(2γ) and the NaI(1γ)+BGO(1γ) are given in comparison. Each column for specific N_{ch} gives $B(\bar{p}p \to \eta M)$ deduced from the monochromatic peak (or its absence) seen in the N_{ch}-prong spectrum. The last column gives the average over different N_{ch}'s.

Channel	$N_{ch}=0$	2	4	6	Average over N_{ch}
		From NaI(2γ)			
$\bar{p}p \to \eta\phi$	<4.0	a			<4.0
$\bar{p}p \to \eta\eta'$		a	<2.3		<2.3
$\bar{p}p \to \eta\omega$	6.3 ± 3.1	b	4.1 ± 1.7[c]		4.6 ± 1.4
$\bar{p}p \to \eta\rho^0$		8.7 ± 2.0[b]			8.7 ± 2.0
$\bar{p}p \to \eta\rho^0/\omega$		13.2 ± 0.7[b]			13.2 ± 0.7
$\bar{p}p \to \eta\eta$	<0.6[d]	e			<0.6
$\bar{p}p - \eta\pi^0/\gamma$	0.27 ± 0.15				0.27 ± 0.15
		From NaI(1γ)+BGO(1γ)			
$\bar{p}p \to \eta\phi$		<2.8			<2.8
$\bar{p}p \to \eta\eta'$	7.6 ± 9.6	<4.31			<4.3
$\bar{p}p \to \eta\omega$	<15	b	<13		<13
$\bar{p}p \to \eta\rho^0$		11.2 ± 2.7[b]			11.2 ± 2.7
$\bar{p}p \to \eta\rho^0/\omega$		15.7 ± 1.2[b]			15.7 ± 1.2
$\bar{p}p \to \eta\eta$	1.6 ± 0.8	e			1.6 ± 0.8
$\bar{p}p \to \eta\pi^0/\gamma$	0.55 ± 0.59				0.55 ± 0.59

[a]The two-prong spectrum for NaI(2γ) was not used, since the systematic error may be large in fitting the $\eta\phi$ and the $\eta\eta'$ peaks which should sit close to the crest of the spectrum.

[b]The $\bar{p}p \to \eta\rho^0/\omega$ peak in the two-prong spectrum was fitted with a sum of $\eta\rho^0$ and $\eta\omega$ peaks by fixing the $B(\bar{p}p \to \pi^0\omega)$ [see Eq. (6c)] deduced from zero- and four-prong spectra (see the text).

[c]Though this peak is located about 20 MeV above the expected position, it cannot be assigned to any other known mesons of narrow widths but $M=\omega$.

[d]The monochromatic η peak should sit on the shoulder of the zero-prong spectrum (see Fig. 5). Yield estimation may suffer from a large systematic error which should depend on the amount of the $\eta\omega$ peak sitting on the crest of the spectrum. Consequently, taking into account the scattering among various fits, we put an upper limit, which was as large as 5 times the statistical upper limit.

[e]The two-prong spectrum was not used since the $\eta\eta$ peak should be located close to the large $\eta\rho^0/\omega$ peak.

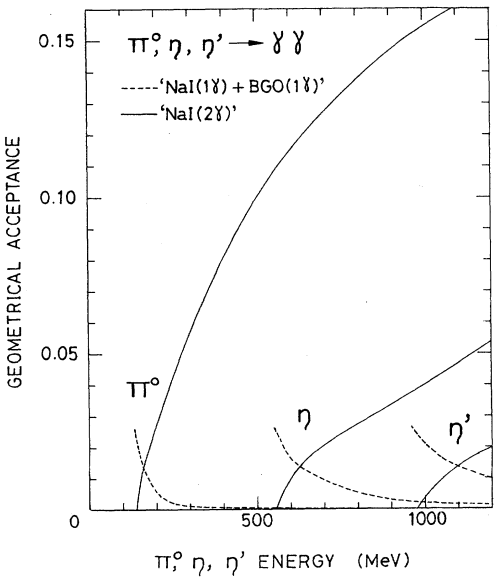

FIG. 8. Geometrical acceptance of π^0, η, and $\eta' \to 2\gamma$ decay for NaI(2γ) (solid curves) and NaI(1γ)+BGO(1γ) (broken ones).

than the sum of those with $m'<4$ according to a phenomenological calculation.[25] Then the yields of $\bar{p}p \to \eta\pi^+\pi^- m\pi^0$ with $m=1$ and 2 can be determined. The yield (uncorrected) summed over $m=1$ and 2 became $(3.74\pm0.30)\%$ with the $\eta\pi^+\pi^-\pi^0/(\eta\pi^+\pi^-\pi^0$

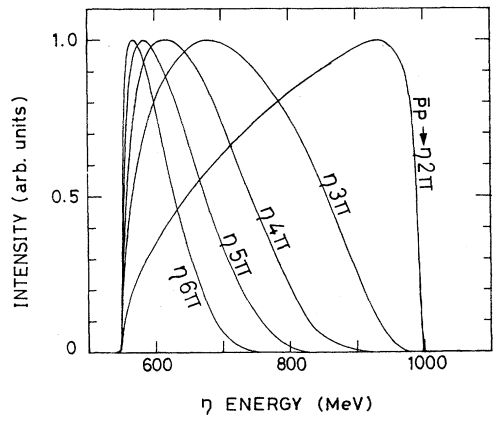

FIG. 9. Energy distribution of η mesons given by the Lorentz-invariant phase space for various pion multiplicities.

TABLE IV. Detection efficiency for $\eta \to 2\gamma$ produced in various annihilation channels of stopping $\bar{p}p$ system. The quoted error is due to an ambiguity in the Monte Carlo calculation.

$\bar{p}p$ annihilation channel	Detection efficiency (%) Geometrical acceptance	Corrected for trigger logic and software cuts
	NaI(2γ) events	
$\eta\pi^0$	4.07	3.58±0.18
$\eta 2\pi^0$	2.92	1.82±0.23
$\eta 3\pi^0$	2.15	0.76±0.08
$\eta\pi^+\pi^-$	2.92	2.40±0.15
$\eta\pi^+\pi^-\pi^0$	2.15	1.08±0.11
$\eta\pi^+\pi^-2\pi^0$	1.60	0.55±0.09
$\eta 2\pi^+2\pi^-$	1.60	0.94±0.14
$\eta 2\pi^+2\pi^-\pi^0$	1.17	0.47±0.09
$\eta 3\pi^+3\pi^-$	0.79	0.39±0.10
	NaI(1γ)+BGO(1γ) events	
$\eta\pi^0$	0.14	0.13±0.01
$\eta 2\pi^0$	0.43	0.28±0.03
$\eta 3\pi^0$	0.68	0.37±0.04
$\eta\pi^+\pi^-$	0.43	0.29±0.02
$\eta\pi^+\pi^-\pi^0$	0.68	0.37±0.04
$\eta\pi^+\pi^-2\pi^0$	0.89	0.41±0.04
$\eta 2\pi^+2\pi^-$	0.89	0.42±0.04
$\eta 2\pi^+2\pi^-\pi^0$	1.08	0.41±0.07
$\eta 3\pi^+3\pi^-$	1.26	0.41±0.07

$+\eta\pi^+\pi^-2\pi^0$) ratio close to unity within a statistical ambiguity of 0.30. Correcting this value for $\gamma \to e^+e^-$, subtracting the contamination of originally zero-pronged events and adding the assumed yield of $\eta\pi^+\pi^-$, we obtained a yield of (5.33±0.50)%,

For $N_{ch}(X)=4$, we neglected $\eta 2\pi^+2\pi^- m\pi^0$ with $m \geq 2$ on the analogy of the small ratio[17,25] of $2\pi^+2\pi^- m'\pi^0$ with $m' \geq 3$ to the sum over $m'=0$, 1 and 2. Attributing the observed events to $\eta 2\pi^+2\pi^-$ and $\eta 2\pi^+2\pi^-\pi^0$, we obtained a total yield (uncorrected) of (1.15±0.12)% with the $\eta 2\pi^+2\pi^-/(\eta 2\pi^+2\pi^- + \eta 2\pi^+2\pi^-\pi^0)$ ratio close to unity within a statistical ambiguity of 0.32. Correcting the above yield for $\gamma \to e^+e^-$ conversion and subtracting the contamination of originally two-pronged events, we obtained a yield of (0.65±0.12)%. An experimental result of $B(\bar{p}p \to \eta 2\pi^+2\pi^-)=(0.6\pm0.2)\%$ given in Ref. 19 is consistent with the above result. For $N_{ch}(X) \geq 6$, we took into account only $\eta 3\pi^+3\pi^-$ channel. Channels of higher multiplicities must be less significant on the analogy of the small ratio[19,25] of $3\pi^+3\pi^- m\pi^0$ with $m \geq 2$ to $3\pi^+3\pi^-\pi^0$. The η yield then becomes (0.03±0.04)% from the slightly ambiguous η peaks seen in the $M(\gamma\gamma)$ spectra.

The yields of $\bar{p}p \to \eta X$ obtained above are summarized in Table VI for each charge multiplicity of X. These quantities have not been published to the authors' knowledge.

TABLE V. Yield of $\bar{p}p \to \eta X$ for various X assuming a single channel dominance in each charge multiplicity (see the text). The result is compared between the two different topologies. The quoted errors are statistical only.

Charge multiplicity $N_{ch}(X)$	Channel ηX	Yield (%)/annihilation NaI(2γ)	NaI(1γ)+BGO(1γ)
0	$\eta\pi^0$	0.36±0.05	1.52±0.40
	$\eta 2\pi^0$	0.71±0.10	0.75±0.20
	$\eta 3\pi^0$	1.72±0.23	0.57±0.15
2	$\eta\pi^+\pi^-$	3.05±0.25	5.71±1.52
	$\eta\pi^+\pi^-\pi^0$	6.78±0.56	4.44±1.18
	$\eta\pi^+\pi^-2\pi^0$	13.32±1.11	4.10±1.19
4	$\eta 2\pi^+2\pi^-$	1.15±0.13	1.13±0.33
	$\eta 2\pi^+2\pi^-\pi^0$	2.29±0.26	1.17±0.33
6	$\eta 3\pi^+3\pi^-$	0.07±0.06	0.00±0.05

C. Inclusive η/π^0 ratio

Summing the values obtained above, we obtained (6.98±0.79)% for the total yield of η in $\bar{p}p$ annihilation at rest. As the π^0 multiplicity per annihilation is 1.9 (Ref. 17), the inclusive η/π^0 ratio becomes $(3.67\pm0.41)\times10^{-2}$, which is statistically much better than a previous experimental result[26] of $\eta/\pi^0=0.05(+0.06, -0.04)$.

D. Inclusive η' production

The yield of η' in $\bar{p}p$ annihilation at rest was estimated from the $\gamma\gamma$ invariant-mass spectrum for the NaI(1γ)+BGO(1γ) topology (see Fig. 10). The detection efficiency for $\eta' \to 2\gamma$ was first calculated for each annihilation channel in $\bar{p}p \to \eta' X$ in the similar way to that for $\eta \to 2\gamma$ in $\bar{p}p \to \eta X$. The detection efficiency for η' was 0.60% for the final state of $\eta'\pi^0$, 0.74% for $\eta' 2\pi^0$, 0.73% for $\eta' 3\pi^0$, 0.75% for $\eta'\pi^+\pi^-$, 0.74% for $\eta'\pi^+\pi^-\pi^0$, 0.69% for $\eta'\pi^+\pi^-2\pi^0$, 0.70% for $\eta' 2\pi^+2\pi^-$, 0.64% for $\eta' 2\pi^+2\pi^-\pi^0$, and 0.58% for $\eta' 3\pi^+3\pi^-$. We assumed the branching ratio into η' plus more than 6π to be small on the analogy[19] of $\bar{p}p \to$ multipions. Though we do not know which channels dominate η' production, all the efficiencies listed above are close to each other. Therefore, we took the mean [(0.66±0.09)%] of the max-

TABLE VI. Yield of $\bar{p}p \to \eta X$ per $\bar{p}p$ annihilation at rest for different charge multiplicities of X. Results from NaI(2γ) and from NaI(1γ)+BGO(1γ) were statistically combined. The numbers of η events are also given. The yield is corrected for contamination of different charge multiplicity caused by $\gamma \to e^+e^-$ conversion and inefficiency in wire planes.

Charge multiplicity $N_{ch}(X)$	Number of observed η NaI(2γ)	NaI(1γ)+BGO(1γ)	Yield (%) per annihilation
0	1487±199	237±63	0.97±0.12
2	8388±696	1897±506	5.33±0.50
4	1238±140	545±155	0.65±0.12
≥6	30±29	1±27	0.03±0.04
Total	11143±1064	2680±751	6.98±0.79

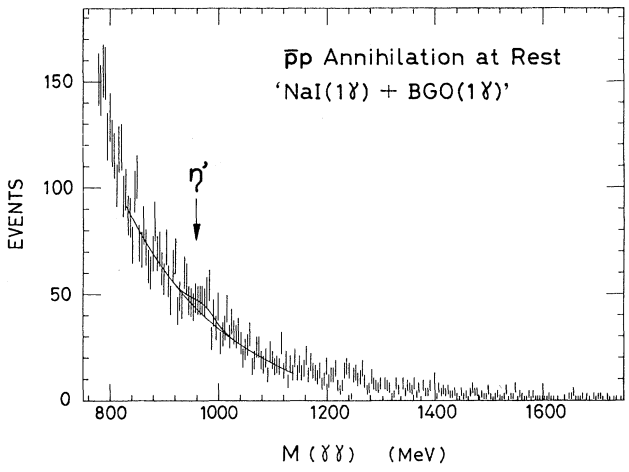

FIG. 10. Invariant-mass spectra of two γ rays above 800 MeV for the NaI(1γ)+BGO(1γ) events. The bin width is 4.16 MeV. The solid curve is a fit with a polynomial background plus a $\eta'(958)$ peak.

imum and the minimum of the above values for the overall detection efficiency of $\bar{p}p \to \eta' X$ with $\eta' \to 2\gamma$ Fit of the η' peak gave a peak area of 67 ± 42 events above the background. The statistical error of the background was by a factor of 1.5 less than the fitting error quoted above. Dividing the peak area by the product of $N_{\bar{p}}$, detection efficiency for η' and $B(\eta' \to 2\gamma)=1.9\%$, we obtained $B(\bar{p}p \to \eta' X)=(1.8\pm1.1)\times10^{-2}$, which gave finally an upper limit of 3.6×10^{-2} at 95% C.L.

Experimental data on η' production in $\bar{p}p$ annihilation at rest are scarce. While Ref. 27 reports a yield of $(3.1\pm0.6)\times10^{-3}$ for an exclusive channel of $\bar{p}p \to \eta'\pi^+\pi^-$ (including $\eta'\rho^0$), the present data seem, according to the authors' knowledge, the first experimental result for the inclusive η' production.

Estimation of $B(\bar{p}p \to \eta' X)$ from the NaI(2γ) sector was not carried out because of a large ambiguity in the detection efficiency for η'; the detection efficiency varies by 2 orders of magnitudes from 0.011% for a high-multiplicity channel of $\eta' 3\pi^+ 3\pi^-$ to 1.92% for a low-multiplicity one of $\eta'\pi^0$.

V. SUMMARY AND DISCUSSION

The result can be summarized as follows.

(i) Yields or upper limits of $\bar{p}p \to \eta M$ for $M=\phi$, η', ω, ρ^0, η, and π^0/γ have been derived from η energy spectra and are given in Eq. (6). $B(\bar{p}p \to \eta\rho^0)$ obtained is close to an experimental value of $(6.9\pm1.4)\times10^{-3}$ given in Refs. 23 and 27 but is larger than $(2.2\pm1.7)\times10^{-3}$ given in Ref. 28. The present result that $\eta\omega$ is less abundant than or comparable to $\eta\rho^0$ [see Eqs. (6c)–(6e)] disagrees with a prediction of the quark rearrangement model of Ref. 2, according to which $\eta\omega$ should be an order of magnitude more abundant than $\eta\rho^0$. An experiment at LEAR by Adiels *et al.*[29] gives a $\eta\omega+\eta\rho^0$ yield compatible with the present result of Eq. (6d) but a $\eta\omega/\eta\rho^0$ ratio different from Eq. (6c).

$B(\bar{p}p \to \eta\pi^0)$ should be approximately equal to $B(\bar{p}p \to \eta\pi^0/\gamma)$, namely, $(2.9\pm1.5)\times10^{-4}$, since $B(\bar{p}p \to \eta\gamma)$ is much smaller [of the order of 10^{-5} (Ref. 30)]. The above value is consistent with $(4.6\pm1.3)\times10^{-4}$ obtained previously by us from measurement of monochromatic π^0 (Ref. 15).

(ii) The yield of $\bar{p}p \to \eta X$ (X denoting anything) per annihilation is $(0.97\pm0.12)\%$ for $N_{\rm ch}(X)=0$, $(5.33\pm0.50)\%$ for $N_{\rm ch}(X)=2$, $(0.65\pm0.12)\%$ for $N_{\rm ch}(X)=4$, and $(0.028\pm0.041)\%$ for $N_{\rm ch}(X)\geq6$. The total yield of η is $(6.98\pm0.79)\%$.

(iii) The inclusive η/π^0 ratio is $(3.67\pm0.41)\times10^{-2}$.

(iv) The yield of $\bar{p}p \to \eta' X$ is less than 3.6% at 95% C.L. Dividing this value by the total η yield given in (ii), we find that the inclusive η'/η ratio is less than 0.52 at 95% C.L.

The systematic error of the yields was about $\pm20\%$, which came partly from the ambiguities in $N_{\bar{p}}$ ($\pm3\%$) as well as in fitting the $M(\gamma\gamma)$ spectra ($\pm2\%$) but mostly from the Monte Carlo calculation of the detection efficiency of η or η' and, for $\bar{p}p \to \eta M$, from the fitting condition for the peaks.

Finally, comparing the present result with the theory, we will give a brief discussion on the dominance of quark annihilation or rearrangement graphs. Furui, Maruyama, and Faesler[31] calculated the inclusive η production in $\bar{p}p$ annihilation at rest in two models of $A3+A2$ and $R3+A2$ in comparison; not $R2$ but $A2$ was adopted since $A2$ gives better agreement in annihilation into two

TABLE VII. Relative branching ratio of $\bar{p}p \to \eta X$ for different charge multiplicities of X is compared between the present result and the calculation by Furui, Maruyama, and Faesler (Ref. 31). The total inclusive branching ratio is also given. The branching ratios were calculated in slightly different prescriptions (a) and (b) (see Ref. 31).

Charge multiplicity $N_{\rm ch}(X)$	Present experiment	Calculations (Ref. 31) $A3+A2$ (a)	$A3+A2$ (b)	$R3+A2$ (a)	$R3+A2$ (b)
0	(13.9 ±1.7)%	10%	13%	16%	11%
2	(76.4 ±7.2)%	84%	77%	68%	70%
4	(9.3 ±1.7)%	5%	10%	16%	19%
≥6	(0.4 ±0.6)%				
$B_{\rm tot}(\bar{p}p \to \eta X)$	(6.98±0.79)%	19.6%	17.6%	7.5%	11.5%

mesons. Table VII compares the branching ratio of $\bar{p}p \to \eta X$ between the calculation and the present experiment. We see that our result favors $A3+A2$ though the yields of zero- and two-pronged events are consistent with the both models. Discrepancy in the total inclusive branching ratio $B_{\text{tot}}(\bar{p}p \to \eta X)$ may not be taken too seriously because, according to the authors of Ref. 31, it has still theoretical uncertainties. As a result, the present experimental result on $\bar{p}p \to \eta X$ favors the $A3+A2$ model to the $R3+A2$ model, though the preference is qualitative.

Dover and Fishbane[5] predicted $R=\bar{\sigma}(\pi^0\eta)/\bar{\sigma}(\pi^0\pi^0)=\frac{1}{25}$ for the rearrangement graph only and order of $\frac{1}{9}$ for the planar graph only, where $\bar{\sigma}(ab)$ is the reduced cross section of $\sigma(\bar{p}p \to ab)/q^{2L+1}$ with q and L the momentum and angular momentum, respectively, in the final state in the c.m. system. The present result of $B(\bar{p}p \to \eta\pi^0)$ discussed above and $B(\bar{p}p \to \pi^0\pi^0)=(2.4\pm0.3)\times10^{-4}$ obtained previously[15] give R of the order of unity for $L=0$ and more than unity for $L=2$. This value is too large to be explained in terms of purely rearrangement graphs, and indicates[5] importance of the annihilation graphs with delicate cancellation and/or of the transition $\bar{N}N \to \bar{\Delta}N$ which feeds only $I=1$, i.e., the $\pi^0\eta$ channel.

According to Genz,[10] the pseudoscalar mixing angle θ_{PS} should satisfy the following equation:

$$[\sin(\theta_0-\theta_{\text{PS}})]^{-2}-1=\bar{\sigma}(\pi^0\eta')/\bar{\sigma}(\pi^0\eta)\ , \tag{8}$$

where $\theta_0=\arctan(1/\sqrt{2})=35.26°$ is the ideal mixing angle. The right-hand term becomes

$$[q(\pi^0\eta)/q(\pi^0\eta')]^{2L+1}B(\bar{p}p \to \pi^0\eta')/B(\bar{p}p \to \pi^0\eta) \tag{9}$$

with $L=0$ ($[q(\pi^0\eta)/q(\pi^0\eta')]^{2L+1}=1.23$) or 2 (2.81) if one of them dominates. Taking $B(\bar{p}p \to \pi^0\eta')=(5.0\pm1.9)\times10^{-4}$ (Ref. 15) and $B(\bar{p}p \to \pi^0\eta)=(3.9\pm1.0)\times10^{-4}$ from statistical average of Eq. (6g) and a result given in Ref. 15, we obtain, from Eq. (8),

$$\begin{aligned} &-12.8° < \theta_{\text{PS}} < 5.4° \quad \text{for } L=0\ , \\ &-0.4° < \theta_{\text{PS}} < 14.9° \quad \text{for } L=2\ . \end{aligned} \tag{10}$$

The theoretically preferred value of $\theta_{\text{PS}}=(-11.1\pm0.2)°$ (Ref. 10) obtained from the quadratic version of the mass formula is in agreement with the $L=0$ case. Improvement in the accuracy of $B(\bar{p}p \to \pi^0\eta)$ and $B(\bar{p}p \to \pi^0\eta')$ is important to make more definite comparison.

ACKNOWLEDGMENTS

The authors are deeply thankful to Professor T. Nishikawa, Professor S. Ozaki, Professor H. Sugawara, and Professor H. Hirabayashi for supporting the present study. They are indepted to many people, especially to the staff of the Proton Synchrotron for the success of the experiment and that of the computer center for help in carrying out analysis. The authors deeply thank Professor L. Tauscher for enlightening discussions.

*Present address: Kochi Medical School, Nankoku, Kochi 781-51, Japan.

†Present address: National Laboratory for High Energy Physics (KEK), Tsukuba, Ibaraki 305, Japan.

[1]H. Rubinstein and H. Stern, Phys. Lett. **21**, 447 (1966); J. Harte, R. Socolow, and J. Van der Meulen, Nuovo Cimento **49**, 555 (1967).

[2]M. Maruyama and T. Ueda, Prog. Theor. Phys. **73**, 1211 (1985).

[3]S. Furui, A. Faessler, and S. B. Khadkikar, Nucl. Phys. **A424**, 525 (1984).

[4]M. Maruyama, S. Furui, and A. Faesler, Nucl. Phys. **A472**, 643 (1987).

[5]C. B. Dover and P. M. Fishbane, Nucl. Phys. **B244**, 349 (1984).

[6]H. Genz, Phys. Rev. D **28**, 1094 (1983); **31**, 1136 (1985).

[7]U. Hartmann, E. Klempt, and J. G. Korner, Phys. Lett. **155B**, 163 (1985).

[8]C. B. Dover, P. M. Fishbane, and S. Furui, Phys. Rev. Lett. **57**, 1538 (1986).

[9]S. Furui, Z. Phys. A **325**, 375 (1986).

[10]H. Genz, Phys. Rev. D **28**, 1094 (1983).

[11]M. Chiba *et al.*, Phys. Lett. B **177**, 217 (1986).

[12]M. Kobayashi *et al.*, Nucl. Instrum. Methods **A245**, 59 (1986).

[13]J. Iwahori *et al.*, Nucl. Instrum. Methods **A245**, 309 (1986).

[14]M. Chiba *et al.*, Phys. Rev. D **36**, 3321 (1987).

[15]M. Chiba *et al.*, Phys. Rev. D **38**, 2021 (1988).

[16]F. James and M. Roos, Computer Phys. Commun. **10**, 343 (1975).

[17]G. Backenstoss *et al.*, Nucl. Phys. **B228**, 424 (1983).

[18]S. Okubo, Phys. Lett. **5**, 165 (1963); G. Zweig, CERN Reports Nos. TH-401 and TH-412, 1964 (unpublished); J. Iizuka, Prog. Theor. Phys. Suppl. **37-38**, 21 (1966).

[19]R. Armenteros and B. French, in *High Energy Physics,* edited by E. H. S. Burhop (Academic, New York, 1969), Vol. IV, p. 237.

[20]M. Chiba *et al.*, Phys. Lett. B **202**, 447 (1988).

[21]S. Devons *et al.*, Phys. Rev. Lett. **27**, 1614 (1971).

[22]S. Devons *et al.*, Phys. Lett. B **47**, 271 (1973).

[23]P. Espigat, C. Ghesquiere, E. Lillestol, and L. Montanet, Nucl. Phys. **B36**, 93 (1972).

[24]$B(\bar{p}p \to \eta\pi^+\pi^-)=(1.2\pm0.3)\%$ from C. Baltay *et al.*, Phys. Rev. **145**, 1103 (1966), and $(1.9\pm0.6)\%$ from Ref. 19.

[25]C. Ghesquiere, in *Proceedings of the International Symposium on $\bar{N}N$ Interaction,* Liblice-Prague, Czechoslovakia, 1974, edited by L. Montanet (CERN Report No. 74-18), p. 436.

[26]G. Levman, R. Singer, and T. Fields, Phys. Rev. D **21**, 1 (1980).

[27]M. Foster *et al.*, Nucl. Phys. **B8**, 174 (1968).

[28]C. Baltay *et al.*, Phys. Rev. **145**, 1103 (1966).

[29]L. Adiels *et al.*, CERN Report No. CERN-EP/88-142 (unpublished).

[30]B. Delcourt, J. Layssac, and E. Polaquier, in *Proceedings of the Workshop on Physics at LEAR with Low Energy Cooled Antiprotons,* Erice, Italy, 1982, edited by Ugo Gastaldi and Robert Klapisch (Ettore Majorana International Science Series: Physical Sciences, Vol. 17) (Plenum, New York 1984), p. 305.

[31]S. Furui, M. Maruyama, and A. Faesler, in *Hadron '87,* proceedings of the Second International Conference on Hadron Spectroscopy, Tsukuba, Japan, 1987, edited by Y. Oyanagi, K. Takamatsu, and T. Tsuru (KEK, Tsukuba, 1987), p. 483.